journal of the mechanical behavior of biomedical materials 153 (2024) 106489

Contents lists available at ScienceDirect

Journal of the Mechanical Behavior of Biomedical Materials

journal homepage: www.elsevier.com/locate/jmbbm

Impact of prior axonal injury on subsequent injury during brain tissue stretching – A mesoscale computational approach

Amirhamed Bakhtiarydavijani [a,*], Tonya W. Stone [a,b]

[a] Center for Advanced Vehicular Systems, Mississippi State University, Starkville, MS, 39759, USA
[b] Department of Mechanical Engineering, Mississippi State University, Mississippi State, MS, 39762, USA

ARTICLE INFO

Keywords:
Traumatic brain injury
Finite element
Axonal injury
Glial scar
Repetitive head impact

ABSTRACT

Epidemiology studies of traumatic brain injury (TBI) show individuals with a prior history of TBI experience an increased risk of future TBI with a significantly more detrimental outcome. But the mechanisms through which prior head injuries may affect risks of injury during future head insults have not been identified. In this work, we show that prior brain tissue injury in the form of mechanically induced axonal injury and glial scar formation can facilitate future mechanically induced tissue injury. To achieve this, we use finite element computational models of brain tissue and a history-dependent pathophysiology-based mechanically-induced axonal injury threshold to determine the evolution of axonal injury and scar tissue formation and their effects on future brain tissue stretching. We find that due to the reduced stiffness of injured tissue and glial scars, the existence of prior injury can increase the risk of future injury in the vicinity of prior injury during future brain tissue stretching. The softer brain scar tissue is shown to increase the strain and strain rate in its vicinity by as much as 40% in its vicinity during dynamic stretching that reduces the global strain required to induce injury by 20% when deformed at 15 s^{-1} strain rate. The results of this work highlight the need to account for patient history when determining the risk of brain injury.

1. Introduction

Research has shown that individuals with a prior history of traumatic brain injury (TBI) are three times as likely to experience another TBI with outcomes expected to be worse than the original TBI (Annegers et al., 1980; Dams-O'Connor et al., 2013a). One study on high school and college football athletes found that 59% of head injuries occurred in athletes with a prior head injury, with 71% of these head injuries occurring in the same season (B.P. Boden et al., 2007). Further repetitive head insults have been assumed to have cumulative effects, with the disease progressing in professional athletes beyond retirement (Hay et al., 2016; Kiernan et al., 2015; McKee et al., 2013, 2016; Mez et al., 2017; Omalu et al., 2005). Considering the results of these epidemiology and pathology studies of TBI, it is imperative that the history effects of prior TBI be considered in current head insult incident assessments.

Early animal surrogate studies of head insults and concussion (Fallenstein et al., 1969; Pudenz and Shelden, 1946) pointed to brain "motion" as a potential cause of concussions. Those early works motivated the study of brain tissue mechanical properties such as its viscoelasticity, hyperelasticity and deformation rate dependency among other things to better understand brain deformation (Franceschini et al., 2006; Rashid et al., 2012, 2013, 2014). Following these advances, computational head models were developed using finite element (FE) methods that allowed the modeling of head impact scenarios. Through these simulations brain injury criteria based on head angular rotations and accelerations (Zhang et al., 2004) and brain tissue stresses, strains, and strain rates (Hajiaghamemar et al., 2020; Hajiaghamemar and Margulies, 2020; Sahoo et al., 2016) were developed. A review of brain injury criteria has been published here (Tse et al., 2015). Another approach is the in vitro testing of neuronal cell cultures under different strain and strain rates to determine axonal injury thresholds (Bar-Kochba et al., 2016; KURTOGLU et al., 2017; Li et al., 2019). These injury criteria are now readily used in FE head impact simulations to determine the risk of injury during head insults (Perkins et al., 2022, 2023). Some recent efforts have also looked to determine neuronal injury thresholds from the subcellular components using computational models. These works have focused on molecular dynamics simulations of neuronal cell components to identify pathophysiological injury pathways (Bakhtiarydavijani et al., 2019; Murphy et al., 2018; A.T.N. Vo et al., 2023; Anh T N Vo et al., 2023). More recent work on brain injury modeling, especially those

* Corresponding author.
E-mail address: ab3447@msstate.edu (A. Bakhtiarydavijani).

https://doi.org/10.1016/j.jmbbm.2024.106489
Received 3 November 2023; Received in revised form 24 February 2024; Accepted 26 February 2024
Available online 27 February 2024

motivated by chronic traumatic encephalopathy and its relation to repetitive head insults, point to the need for a history dependent brain injury or damage model (Horstemeyer et al., 2019; Noël and Kuhl, 2019) that addresses the evolution of brain injury through multiple head insults. In this regard, cyclic tensile-compression testing of brain tissue shows mechanical behavior does not deteriorate even for cyclic deformations of up to 40% stretch (Franceschini et al., 2006). This is while tensile strains as low as 0.10, in high enough strain rate, have been seen to induce brain injury (Giordano and Kleiven, 2014). In regards to injury evolution, cell culture studies have shown that cell response to the mechanical load evolves in the time scale of hours even after high-rate deformations (Bar-Kochba et al., 2016; Johnson et al., 2013; LaPlaca and Thibault, 1997; Li et al., 2019). This means that brain injury models, and especially those for repetitive head impact modeling, should consider the temporal evolution of neuro-pathophysiology and the effects of prior head impacts on their injury prediction.

Diffuse axonal injury, more accurately described as multi-focal axonal injury, is one of the most common neuropathological consequences of closed head TBI, especially in lower severity TBI (Johnson et al., 2013). Axonal injury occurs when large rotational accelerations, due to an impactor or inertial forces, are imposed on the head and thus brain tissue. In the soft brain tissue, these rotational accelerations translate into the stretching and shearing of the axons. Here, cell culture studies show axons over-stretched at sufficiently high strain rates may be injured (Pfister et al., 2003; Singh et al., 2009; Skotak et al., 2012). While larger stretches can tear the axon completely, lower magnitudes of stretching may disrupt the cub-cellular cytoskeletal microtubules and the axonal membrane. In the axonal cytoskeleton, the microtubule-associated protein tau that binds the microtubules (Binder et al., 1985; Black et al., 1996) is susceptible to overstretching (Ahmadzadeh et al., 2014; Tang-Schomer et al., 2010), in a rate dependent manner (Ahmadzadeh et al., 2014; Kant et al., 2021), as the tau protein is significantly smaller than the microtubules it connects. After over-stretching, as shown by amyloid precursor protein immunoreactivity that is transported by fast axonal transport, transfer material begins to accumulate locally resulting in swelling within a few hours (Johnson et al., 2013; Tang-Schomer et al., 2010). Following injury local axonal swelling and degradation may occur. Axonal swelling, blebbing, and loss of cross-section are some of the pathophysiologies used to determine critical axonal stretching thresholds (Bain and Meaney, 2000; Pfister et al., 2003; Singh et al., 2009; Skotak et al., 2012). As the axons begin to degrade, glial cells are attracted to the site (Bardehle et al., 2013; Wang et al., 2018) to clean up the degrading axons and prevent further deleterious effects on neighboring brain cells. This clean-up process is accompanied by glial scar development (Rolls et al., 2009). However, these scars prevent the regeneration of brain tissue and axonal regrowth (Asher et al., 2001; Faulkner et al., 2004; Fawcett and Asher, 1999; Rolls et al., 2009). A recent study has shown that the glial scar tissue is significantly softer than the surrounding tissue (Moeendarbary et al., 2017). The effects of axonal degradation and the resulting formation of softer glial scar tissue on future head insult-related injury remains to be determined and is a focus of this study.

The goal of this work is to determine whether prior axonal injury and glial scar formation in the brain tissue can facilitate future axonal injury from a mechanical standpoint. We hypothesize that tissue softening as a result of axonal degradation and glial scar formation can facilitate axonal injury during future tissue deformations. To assess this hypothesis, we use mesoscale computational models of brain tissue consisting of healthy and injured tissue. A novel neuropathology-based injury model is then developed to capture injury threshold and evolution. The axonal critical stretch threshold (ACST) is determined considering the axonal stretch and stretch rate history based on molecular dynamics studies of microtubules (Ahmadzadeh et al., 2014) and cell culture results (Skotak et al., 2012). The mechanical effect of the ensuing axonal degradation and scar formation (Moeendarbary et al., 2017) is determined using a temporally evolving damage model. The mesoscale computational models of brain tissue are then used to determine the effects of prior axonal injury and damage evolution during future brain tissue stretching. To the extent of the authors' knowledge this is the first pathophysiology-based brain injury model implemented that captures the history of injury.

2. Methods

2.1. Constitutive material model

A constitutive material model is developed at the mesoscale to capture the mechanical response of the brain tissue subjected to injury. The mechanical response of the brain tissue is assumed to be hyperelastic and viscoelastic with a damage evolution term that captures the effect of axonal injury on the mechanical response. A unique history, deformation, and deformation rate dependent axonal injury threshold is developed to determine when axonal injury has occurred. We note that the term "damage" herein refers to the effect of injury evolution on tissue stiffness. Finally, it should be noted that scalar variables are written in italic (such as λ) while tensors are written in bold (such as $\boldsymbol{\sigma}$).

2.1.1. Mechanical constitutive model

The brain's response to mechanical loads is determined using a first-order Ogden hyperelastic material model with a second-order Prony series viscoelastic model. The strain energy, W, is described by:

$$W = \frac{\mu_p}{\alpha}\left(\lambda_1^{\alpha} + \lambda_2^{\alpha} + \lambda_3^{\alpha} - 3\right) + \frac{1}{C}(J-1), \quad [1]$$

where λ_i are the principal strains, J is the second invariant of the deviatoric stress tensor, and α is a material constant. Material constants C and μ_p are calculated by

$$C = \frac{2}{K} = \frac{3(1-2\nu)}{\mu_0(1+\nu)}, \mu_p = \frac{\mu_0\alpha}{2}(1-D), 0 \le D < 1\,. \quad [2]$$

Here, K is the bulk modulus, μ_0 is the initial shear modulus, ν is the Poisson's ratio, and D is the mechanical effects of axonal injury and scaring. The hyperelastic principal stresses are then calculated through:

$$\sigma_j = \lambda_i \frac{\partial W}{\partial \lambda_j} - p \quad [3]$$

with p being the hydrostatic pressure. The viscoelastic response $G(t)$ is determined by:

$$G(t) = 1 - \sum_{i=1}^{2} g_k \left[1 - \exp\left(-\frac{t}{\tau_k}\right)\right], \quad [4]$$

where, g_k is the loss modulus, t is time, and τ_k is the decay time. The stress in the current time is then defined as a function of the current hyperelastic stress, $\boldsymbol{\sigma_0}$, the history response of the rate of the loss modulus, $\dot{G}$, and the hydrostatic pressure:

$$\boldsymbol{\sigma}(t) = \boldsymbol{\sigma}_0(t) + \frac{1}{G_0}\int_0^t \dot{G}(t')\boldsymbol{\sigma}_0(t-t')dt' + \mathbf{I}p. \quad [5]$$

Here $\boldsymbol{\sigma}(t)$ is the current stress tensor, $\boldsymbol{\sigma}_0(t)$ is the hyperelastic stress tensor, and $\mathbf{I}$ is the identity tensor. The integration accounts for the viscoelastic relaxation of the material considering its deformation history.

2.1.2. Glial scarring model

The process of glial scar formation is a two-step phenomenon that can be initiated by axonal injury. Following the initial injury, axonal degradation can occur (Moeendarbary et al., 2017). This is followed by the clean-up process and the removal of axonal myelin sheaths (Fawcett

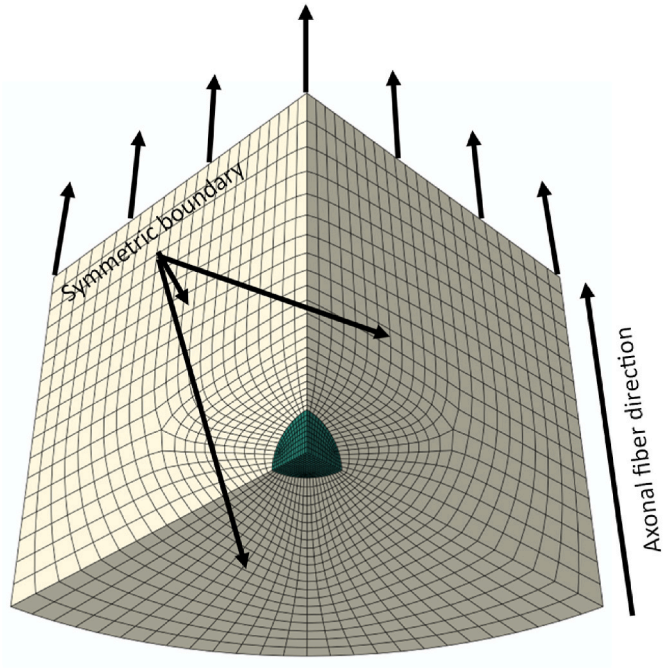

Fig. 1. One-eighth symmetry meshed mesoscale brain tissue model with light gray healthy tissue (section 1) and dark green scar tissue (section 2). This model has a radius of 2 mm and height of 2 mm.

and Asher, 1999) that affect tissue stiffness. This process occurs in the hours following the initial insult reducing the modulus by three-fold (Moeendarbary et al., 2017). As glial scars begin to form, brain tissue then slowly recovers some of its mechanical strength, with the elastic modulus increasing from day 9 to day 21 (Moeendarbary et al., 2017). As scarring blocks the reconnection of axons and the development of myelin sheets, it can be inferred that tissue stiffness does not fully recover but further study for longer time frames is required. Based on the mentioned prior clinical and molecular dynamics studies of axonal injury, an axon critical stretch threshold (ACST), Φ_{crit}, is defined in the rate form considering its strain rate dependence:

$$\Phi_{crit} = \int_{t_0}^{t_1} \dot{\Phi}_{crit} dt, \dot{\Phi}_{crit} = a_1 \left(1 - a_2 \exp\left(-\frac{\dot{\varepsilon}_l}{a_3}\right)\right) \dot{\varepsilon}_l, \Phi_{crit\,t=0} = -a_4. \quad [6]$$

where $\dot{\varepsilon}_l$ is the magnitude of the Lagrangian axonal strain rate calculated from the local strain, a_1, a_2, a_3, and a_4 are constants and dt is the time increment. Here the first term addresses the effect of strain and strain rate on straining the microtubule and tau cleavage, while the second term ($a_4 dt$) is a slow relaxation that relates to the possible slow tau protein creep. Once the ACST is achieved, the mechanical properties evolve, or degrade and recover, with the axonal degradation and scar formation:

$$D = \left[D_0\left(1 - \exp\left(-\frac{t_{inj}}{\tau_{inj}}\right)\right) - D_1\left(1 - \exp\left(-\frac{t_{inj}}{\tau_{rec}}\right)\right)\right], \quad [7]$$

$$0 < D_1 < D_0 < 1, 0 < \tau_{inj} < \tau_{rec}. \quad [8]$$

Here the term $D_0(1 - \exp(-t_{inj}/\tau_{inj}))$ captures the softening of the mechanical properties due to axonal degradation and the term $D_1(1 - \exp(-t_{inj}/\tau_{rec}))$ captures the scar formation. D_0 and D_1 are the axonal injury and scarring stiffness-related constants, respectively. τ_{inj} and τ_{rec} are the half-life of axonal degradation and scar development, respectively, and t_{inj} is the time passed after ACST is first achieved.

Our custom constitutive material model is implemented in a VUMAT user subroutine in Abaqus SIMULIA 2020; Smith (2020). In short,

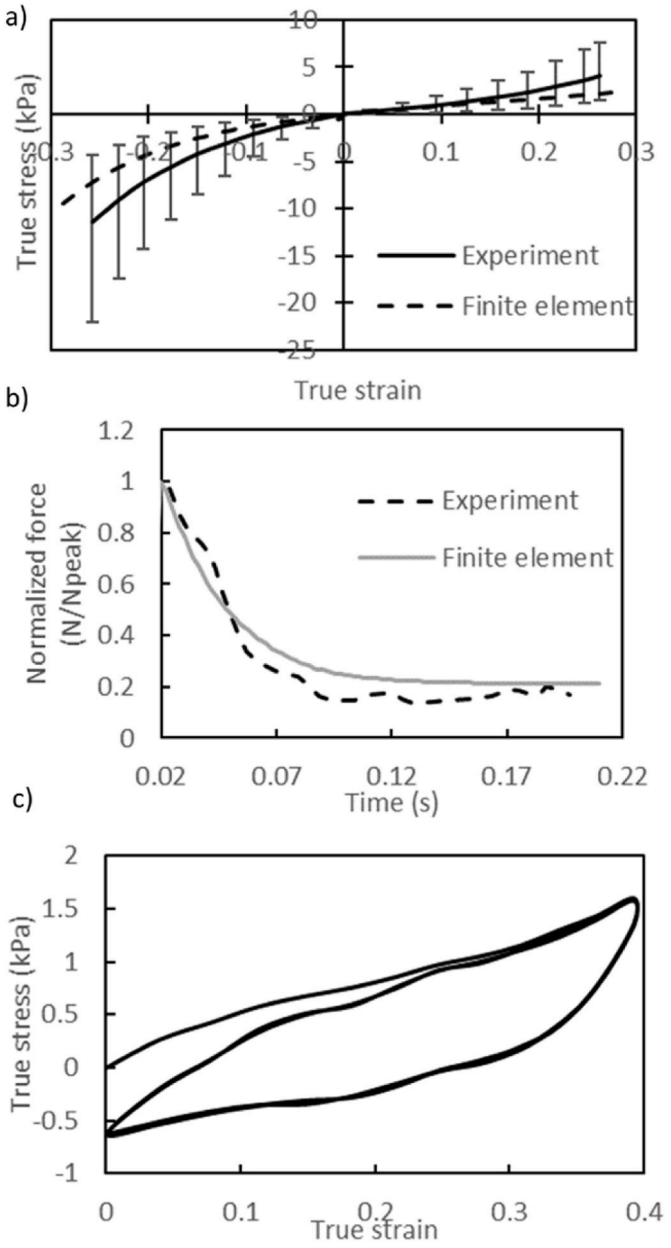

Fig. 2. Calibration of material model stress-strain curves for brain tissue deformed at 30 s^{-1} strain rate to experimental data of porcine tissue (Rashid et al., 2012, 2013, 2014) in a) tension-compression, b) relaxation, and c) three cyclic tensile load-unload (only model response).

Equation (6) determines when axons are injured, Equation (8) defines the damage that feeds into the mechanical response of the tissue. The mechanical response of the tissue is then determined with Equation (5) informed by equations (4) and (2).

2.2. Finite element models

All simulations were performed in Abaqus SIMULIA 2020 in dynamic explicit with no modifications to the linear and quadratic bulk viscosity. Models used for calibration were deformed at 30 s^{-1} with no mass scaling. Models used to study the phenomenon were deformed at 15 s^{-1}, 1.0 s^{-1}, and 0.1 s^{-1} strain rates, with 1.0 s^{-1} and 0.1 s^{-1} using 1000 and 3000 mass scaling, respectively. These strain rates were chosen to consider injury strain rate dependency seen in experimental data (see section 2.2.1).

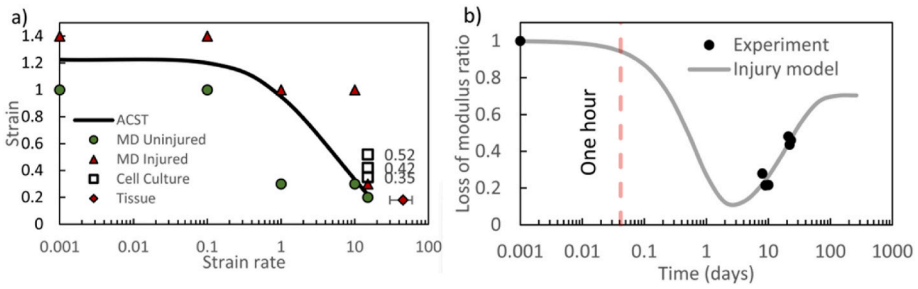

Fig. 3. a) Injury threshold (ACST) calibration for equation (7) (black line) to molecular dynamics simulations of tau breakage (Ahmadzadeh et al., 2014) under tensile strain. Green circle and red triangle represent undamaged and damaged microtubule connections derived from molecular dynamics simulation results. The squares represent cell culture risk of axonal injury based on the strain and strain rate magnitude (Skotak et al., 2012) and the diamond represents a tissue injury threshold from the optic nerve (Bain and Meaney, 2000). The provided data point labels with the cell culture data (square) show percentage of dead cells based on the strain and strain rate magnitude. b) Mechanical injury softening (equation (8)) calibrated to scar stiffness (Moeendarbary et al., 2017). The experimental data show that after the initial injury brain tissue regains some of its stiffness as scar tissue forms (see section 2.1.2).

Table 1
Material constants for the mesoscale hyperelastic viscoelastic constitutive material model with secondary injury.

Hyperelasticity	μ_p (MPa)	α	C	
	0.0036	−8.701	100	
Viscoelasticity	G_1	G_2	τ_1	τ_2
	0.5837	0.2387	0.02571	0.0257
ACST	a_1	a_2 (1/s)	a_3	a_4
	2.8212	0.7089	9.2139	0.01
Injury evolution	D_0	τ_{inj} (s)	D_1	τ_{rec} (s)
	0.995767	60000	0.7	1858227

The models used to calibrate the mechanical responses under uniaxial tension, uniaxial compression, uniaxial tension-relaxation, and cyclic loading all use a one-eighth cylindrical model with a 7.5 mm radius and 10 mm height that is meshed with 540 C3D8R elements. The shear state calibration uses a rectangular 19 by 19 mm cross-section with a height of 4 mm, which is meshed with 2880 C3D8R elements. These dimensions relate to the works of Rashid et al. (Rashid et al., 2012, 2013, 2014) whose work is used to calibrate the mechanical behavior of the material model at dynamic strain rates.

A mesoscale finite element model is developed to study the effects of the axonal injury site. This model is a one eighth symmetric with a radius of 2 mm and a height of 2 mm with 11500 C3D8R elements. The initial scar is assumed to have a radius of 0.1 mm (Fig. 1). Considering the model size, the direction of the axons is assumed to uniformly align with the Y direction, that is the same as the loading direction.

2.2.1. Model calibration

The material model of the healthy brain tissue is calibrated for tensile (Rashid et al., 2014), shear (Rashid et al., 2013), and compressive (Rashid et al., 2012) tests performed at 30 s^{-1} strain rate (Fig. 2). The viscoelastic relaxation response was also calibrated to tensile tests (Rashid et al., 2014) performed at 30 s^{-1} strain rate (Fig. 2).

The axonal injury threshold ACST (Fig. 3a) in equation (7) is calibrated to tau cleavage during tension (Ahmadzadeh et al., 2014). The work of Ahmadzadeh is quantified to determine a 50% chance of injury where the values for injury are determined by the midway point between uninjured and injured (black line in Fig. 3a). The injury evolution is directly calibrated with Moeendarbary (Moeendarbary et al., 2017) (Fig. 3b) results that are normalized by the initial modulus.

The material constants for the calibrated hyperelastic viscoelastic constitutive model with secondary injury are presented in Table 1. Here, the hyperelastic and viscoelastic material properties are determined by optimizations shown in Fig. 2. ACST constants in Table 1 are determined from Fig. 3 a, and injury evolution are determined from Fig. 3 b. $\Phi = 0.5$ is the critical value for the ACST whereby the axon is assumed to be injured.

After the ACST is achieved the mechanical properties of the injured tissue evolve temporally (Fig. 4a) with the evolution of injury. As the axons begin to degrade the tissue modulus is reduced, (Fig. 4b); However as the glial scars begin to form, the tissue starts to regain some of its stiffness (Fig. 4b) (Moeendarbary et al., 2017).

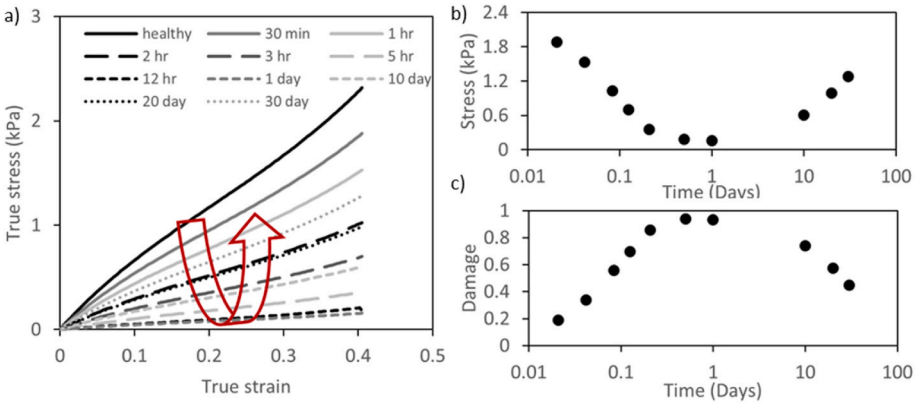

Fig. 4. The effect of axonal degradation and scar formation (with time) on the tissue mechanical response when stretched at 15 s^{-1} strain rate. a) stress-strain curves of tensile test after initial scarring where the red arrow shows the softening and stiffening of the tissue post injury time, b) true stress at 0.4 true strain versus post-injury time, and c) Damage at 0.4 true strain versus post-injury time. These results are from a whole injured computational model where sections 1 and 2 in Fig. 1 are both defined as injured tissue.

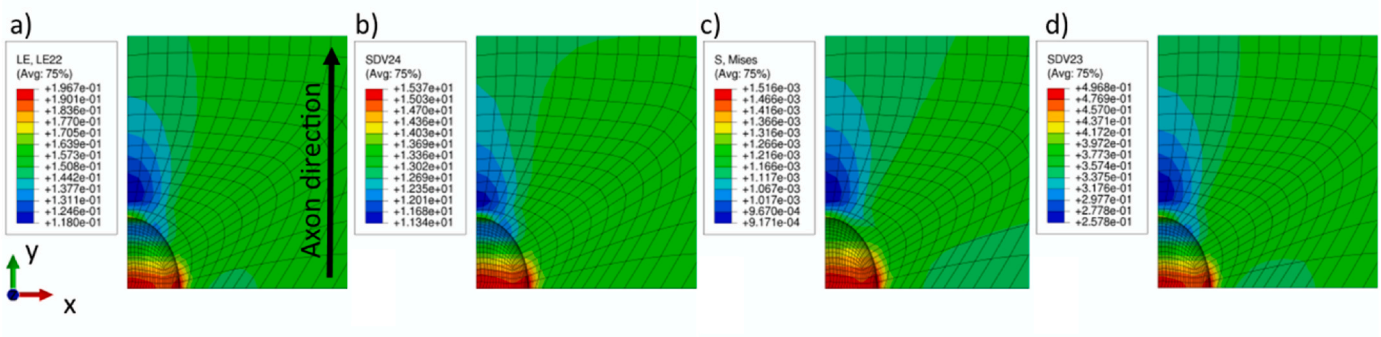

Fig. 5. Side view of model (Fig. 2) results after 0.151 global strain at 15 s-1 strain rate under uniaxial tension close to the scar tissue (hidden): a) Axonal strain, b) axonal strain rate c) von Mises stress, and d) ACST. The scar mechanical properties correlate to 1 day post initial injury (D~ = 0.8) and at the time of injury initiation (Fig. 5 a.).

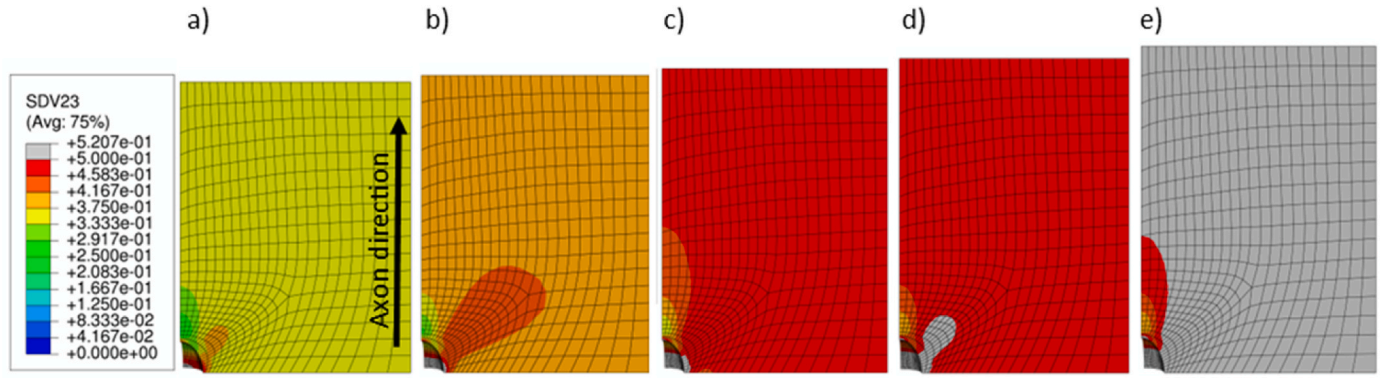

Fig. 6. The evolution of ACST in the vicinity of a scar with 0.8 damage pulled at 15 s-1 strain rate where 0.5 is the injury threshold. The global strain on the mesoscale tissue models from left to right are: a) 0.151, b) 0.174, c) 0.197, d) 0.207, and e) 0.217. Note that the scar is hidden, and a surface cut is shown to facilitate visualization.

3. Results

A mesoscale model of brain tissue with an injured site (Fig. 1) with a novel axonal injury threshold (ACST), Eq. (7), and injury evolution, Eq. (8), is used to study the effects of axonal degradation and scar tissue formation on tissue stretching. The model is then pulled at different strain rates and considering different rest times after injury to determine susceptibility to future injury.

Fig. 5 shows brain tissue model with an initial one-day old, injured site (that is hidden for better visualization) that is pulled to 0.15 true strain in tension at 15 s^{-1} strain rate. The existence of a softer injured tissue in the model is shown to increase the axonal strain, axonal strain rate, and von Mises stress locally as shown in Fig. 5a-c, respectively. The increases in axonal strain and strain rate cause the injury threshold to accumulate much faster in the vicinity of the scar (Fig. 5d).

Fig. 6 shows the ACST evolution in a model with an initial one day old injured site pulled in tension at 15 s^{-1} strain rate. The axonal injury threshold is achieved after 0.151 global strain, adjacent to the axonal scar. The injury threshold in the rest of the tissue (far away from the injured tissue) stays uniform until it is achieved in most of the model when global strain reaches 0.217.

Fig. 7 a. and b. show the local strain and local strain rate, normalized by the global strain, vs the global strain and their evolution considering their distance from the scar, respectively. In these figures the 0 legend refers to brain tissue on the scar surface, while 1 refers to a distance of 1 scar radius from the scar surface. It is seen that both normalized strain and normalized strain rate are highest at the scar interface with a value of 1.4 for both strain and strain rate. Both strain and strain rate ratios decrease toward 1 as we move away from the scar and as higher strains are achieved in the tissue.

The strain rate dependence of the axonal injury initiation for mesoscale tissue models with and without a scar is summarized in Table 2 where the global strains are calculated from the displacement of the top node of the model (Fig. 1). This injury mechanism is seen to be very strain rate dependent where at 0.1 s^{-1} strain rate with a preexisting scar, 0.41 axonal strain is required to trigger injury while at 15 s^{-1} strain rate only 0.16 axonal strain is required. The global strains required for the injury threshold to be achieved considering damage in an element of the model are then presented in Table 3.

Fig. 8 presents the effect of damage magnitude on the local normalized strain profile, that is the local strain normalized by the global strain, for global strains from 0.05 (Fig. 8a) to 0.3 global true strain (Fig. 8f) for a model pulled at 15 s-1 strain rate. It is seen that the higher the magnitude of damage, or the softer the injured tissue, the higher the strain localization. Again, it is seen that the local increases in the axonal strain because of the scar are reduced at larger strains. It should be noted that the effective radius of the scar seems to be independent of the global true strain.

Fig. 9 shows the effect of scar size on the normalized local strain profile. The radius of the scar in Fig. 1 was increased by 1.5 and 2 times. The models were then stretched to 0.1 strain at a 15 s^{-1} strain rate. The strain profile at the vicinity of the scar and perpendicular to the stretching direction was then normalized by the global strain (0.1 strain) and was plotted considering the distance from the scar vicinity. It can be seen that the radius through which the scar increases the strain magnitude is 0.4 times the radius of the injury site.

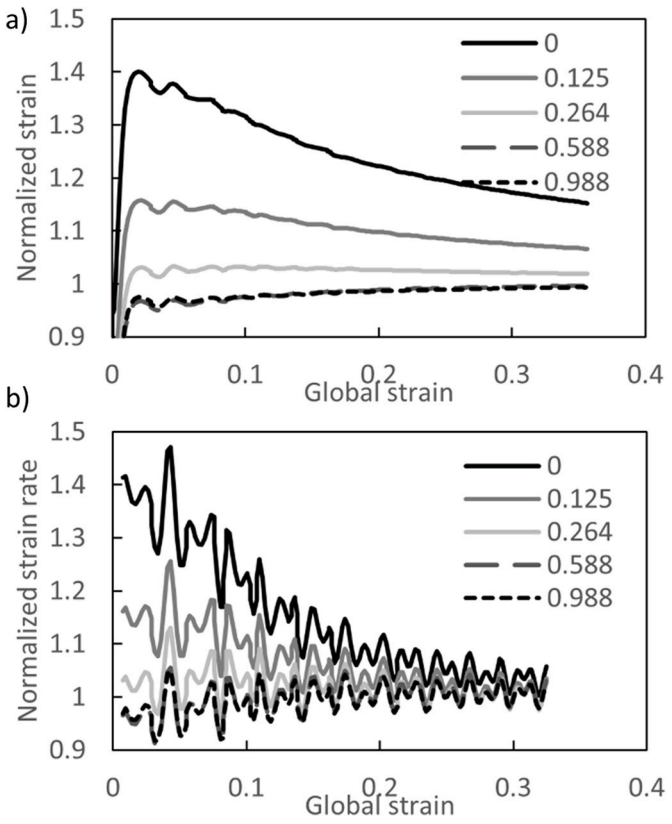

Fig. 7. The effect of a scar on the local axonal strain and local axonal strain rate in the vicinity of the scar in the mesoscale model under uniaxial tension at 15 s^{-1} in the direction of axons. a) local axonal strain normalized by the global strain and b) axonal strain rate normalized by the global axonal strain rate at different normalized distances from the scar with 0 being on the scar-tissue interface, and 1 being a distance of 1 scar radius from the scar surface.

Table 2
Global strain required to initiate or further injury in brain tissue considering strain rate in healthy issue and one day after injury.

Global tensile rate (s^{-1})	Global strain required to induce axonal injury after initial injury	
	Healthy tissue	One day after initial injury (D = 0.8)
0.1	0.554	0.492
1	0.482	0.410
15	0.211	0.160

4. Discussion

In this work, we have identified a pathway through which prior brain injury in the form of axonal injury and the resulting glial scar formation can facilitate injury during future head insults. We show that the existence of prior injury can reduce the global strains (Fig. 7a) required to achieve axonal injury thresholds in its vicinity by as much as 20% (0.20–0.16 global strain, Table 2). This means that head injury thresholds for individuals with a history of TBI may be lower than those without a prior TBI, though macroscale head simulations are required to determine the results more accurately. This finding agrees with prior epidemiology studies that found individuals with a history of TBI are three times as likely to experience another TBI when compared to adults without a history of TBI (Annegers et al., 1980; Dams-O'Connor et al., 2013b). This locally lowered injury threshold may also hint at a mechanism for local injury growth via generally sub injurious/concussive head impacts. Here the strains in the brain from a generally sub-concussive head insults could trigger axonal injury in the vicinity of prior sites of injury.

It was also seen that the effective radius of a scar, that is the radius through which the brain tissue experienced increased strains and strain rates, is independent of scar tissue stiffness (Fig. 8) and is to be directly related to the scar radius (Fig. 9). As the circular effective area of the scar is approximately the square of its radius, the larger the current injury site, the faster injury can grow during the next head insult. Hence when considering multiple head insults, as the number of head insults increases the number of axons injured through this mechanism would grow by the power of two. The progressive nature of this proposed injury growth agrees with epidemiology studies showing individuals with a history of TBI will experience more detrimental consequences with a second TBI incident (Dams-O'Connor et al., 2013b). It should be noted that this high rate of injury growth only occurs when the head insults result in tensile stretching of the axons.

The computational models presented here capture the effects of temporal axonal injury evolution and allow us to study the effects of such injuries during multiple head insults. After an initial injury, the mechanical stiffness of the injured brain tissue evolves. Initially the injured tissue slowly becomes softer. This tissue softening represents the slow degradation of axons. Following the initial tissue stiffness degradation, the tissue recovers some of its stiffness. This recovery of stiffness represents glial scar development (Fig. 4a and 5b). In the meantime, the surrounding healthy tissue retains its stiffness. Because of this difference in stiffness, when tissue that includes an injury site is stretched more of the load is focused on the stiffer healthy tissue (Fig. 5c) in the scar vicinity. The higher loads mean that this healthy brain tissue experiences increased axonal strain (Fig. 5a and Fig. 6a) and strain rate (Fig. 5b and Fig. 6b) on the plane perpendicular to the loading direction when compared to the applied, or global, strain. In this regard, the initial axonal strain and strain rate next to the scar at a global strain rate of 15 s^{-1} is approximately 1.4 times that of the global strain and strain rate (Fig. 8a). While the strain rate does dissipate to global strain rate levels at larger strains, the local strain is still 1.15 times the global strain after 0.3 true strain (Fig. 8f). The reduction of the normalized strain with increasing strain (Fig. 8) may be due to the changes in the material stiffness (hyperelasticity) that is initially nearly constant but increases at larger strains (Fig. 2a). At larger strains, the stiffness of the scar and healthy tissue in its vicinity increases faster than the rest of the model that is at a lower strain magnitude. This mitigates some of the effects of the extra soft scar tissue on strain localization. The collective effect of the increase in the local strain and strain rate is that, when prior injury is present, injury thresholds require smaller global strains (0.16 versus 0.20) to be triggered (Table 3).

A novel framework for mechanically induced axonal injury is presented that includes a history dependent injury threshold or ACST and a temporally evolving pathophysiology-based injury evolution for axonal injury that determines the local mechanical properties of brain tissue and its effects on further injury. In determining the ACST or axonal injury criterion we have used axonal tau cleavage thresholds determined through molecular dynamics simulations (Ahmadzadeh et al., 2014). In comparison other axonal injury criteria have been determined using in

Table 3
Global strain required to induce injury after a previous injury for tissue strained at 15 s^{-1} strain rate for considering different scar tissue damage magnitude.

D	Healthy	0.1	0.2	0.3	0.4	0.5	0.6	0.7	0.8	0.9
ε_{inj}	0.211	0.205	0.201	0.193	0.187	0.180	0.174	0.166	0.160	0.151

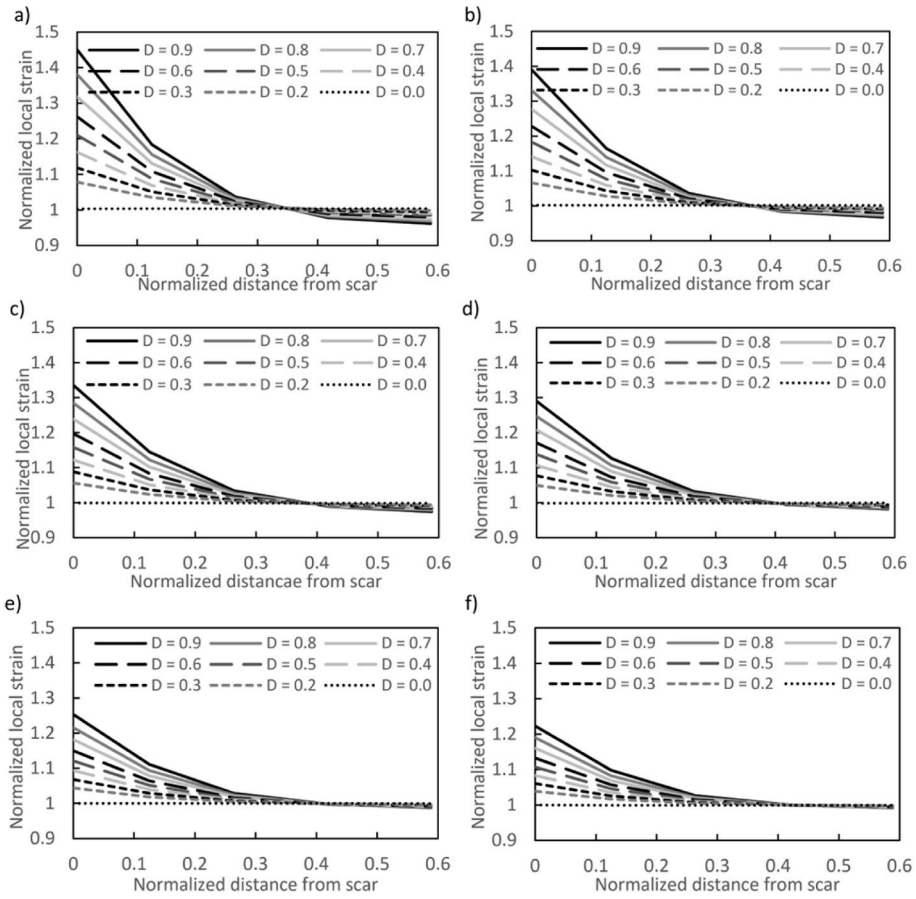

Fig. 8. The effect of tissue stiffness degradation (D) on the strain profile adjacent to a glial scar. Here D = 0 refers to healthy tissue and D = 0.9 refers to a 90% reduction in tissue stiffness from healthy tissue. The figures show the local strain normalized with the global strain considering distance from scar (normalized by scar radius) at the global true strain of a) 0.05, b) 0.10, c) 0.15, d) 0.20, e) 0.25, and f) 0.30.

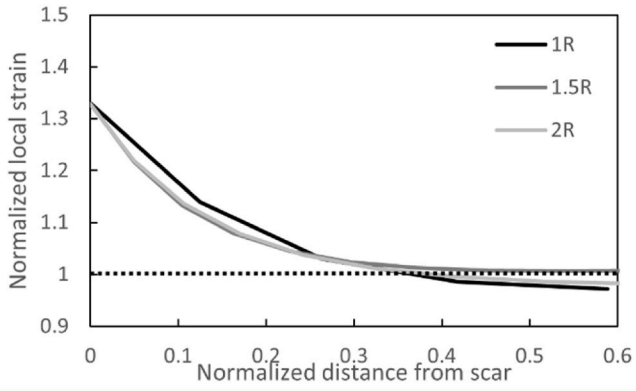

Fig. 9. The independence of normalized strain profile from normalized scar radius. The normalized local strain versus the normalized distance from scar is shown for three different scar sizes with R = 0.1 mm. Note that the distance from scar is normalized by the respective scar radius.

vitro (Bain and Meaney, 2000; Li et al., 2019; Pfister et al., 2003) and FE simulations (Hajiaghamemar et al., 2020; Sahoo et al., 2016). In this regard, the ACST can be calibrated to other axonal injury criteria. This should affect the strain required to injure the tissue but not the strain localization in the scar vicinity. Considering the complexity of this problem, some assumptions have been made to simplify the modeling effort. These include axonal waviness, orientation distribution, and injury threshold variation. As this injury model is developed at the mesoscale where elements at the site of injury are in the tens of microns, axonal waviness and orientation distribution cannot be prescribed at this length scale but will need to be accounted for in organ level (macroscale) models. Further, injury threshold variations because of geometrical and structural differences between axons can also be introduced via statistical means into the macroscale model.

5. Conclusions

In the current work, we used mesoscale FE models to show that prior TBI in the form of axonal degradation and glial scar formation may increase the risk of future brain injury during secondary tissue stretching.

- The existence of the softer injured tissue increases the strain and strain rate in its vicinity, reducing the global strains required to initiate further axonal injury by as much as 20% at higher stretching rates.
- The model predicts that a secondary insult of similar magnitude may be accompanied by a near 2nd order growth of the injured region when compared to the initial insult.
- The magnitude of normalized strain in the vicinity of the scarred tissue is dependent on the loss of tissue stiffness in the scar (Fig. 8 and Table 3) but did not the scar size (Fig. 9).

The novel pathophysiology based axonal injury model presented here captures the initiation of axonal injury, the degradation of tissue, and the temporal evolution of tissue mechanical properties that ensue. Hence this modeling approach is especially useful in determining injury for repetitive head insults when extended to the organ and whole head

models.

CRediT authorship contribution statement

Amirhamed Bakhtiarydavijani: Writing – review & editing, Writing – original draft, Methodology, Investigation, Data curation, Conceptualization. **Tonya W. Stone:** Writing – review & editing, Writing – original draft, Visualization, Supervision, Resources, Methodology, Conceptualization.

Declaration of competing interest

The authors declare that they have no known competing financial interests or personal relationships that could have appeared to influence the work reported in this paper.

Data availability

Data will be made available on request.

Acknowledgement

The authors would like to thank the Center for Advanced Vehicular Systems at Mississippi State University for their support of this work.

Appendix A. Mesh convergence

Mesh size study was performed to confirm convergence using tensile tests at 30 s^{-1} strain rate (Figure A1.). It was found that the force-displacement behavior was stable. The finer mesh with further refined mesh at the scar boundary was chosen to provide more resolution at the scar interface.

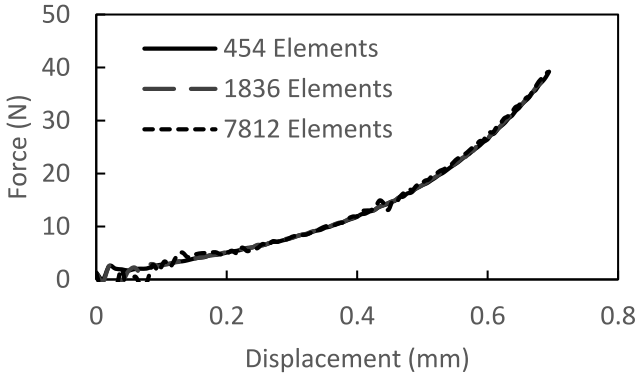

Fig. A.1. Mesh convergence for force-displacement at 30 s^{-1} strain rate.

References

Ahmadzadeh, H., Smith, D.H., Shenoy, V.B., 2014. Viscoelasticity of tau proteins leads to strain rate-dependent breaking of microtubules during axonal stretch injury: predictions from a mathematical model. Biophys. J. 106, 1123–1133. https://doi.org/10.1016/j.bpj.2014.01.024.

Annegers, J.F., Grabow, J.D., Kurland, L.T., Laws, E.R., 1980. The incidence, causes, and secular trends of head trauma in Olmsted County, Minnesota, 1935-1974. Neurology 30, 912–919. https://doi.org/10.1212/WNL.30.9.912.

Asher, R.A., Morgenstern, D.A., Moon, L.D.F., Fawcett, J.W., 2001. Chondroitin sulphate proteoglycans: inhibitory components of the glial scar. Prog. Brain Res. 132, 611–619. https://doi.org/10.1016/S0079-6123(01)32106-4.

Boden, B.P., Tacchetti, R.L., Cantu, R.C., Knowles, S.B., Mueller, F.O., 2007. Catastrophic head injuries in high school and college football players. Am. J. Sports Med. 35, 1075–1081. https://doi.org/10.1177/0363546507299239.

Bain, A.C., Meaney, D.F., 2000. Tissue-level thresholds for axonal damage in an experimental model of central nervous system white matter injury. J. Biomech. Eng. 122, 615. https://doi.org/10.1115/1.1324667.

Bakhtiarydavijani, A., Murphy, M.A., Mun, S., Jones, M.D., Bammann, D.J., Laplaca, M. C., Horstemeyer, M.F., Prabhu, R.K., 2019. Damage biomechanics for neuronal membrane mechanoporation. Model. Simul. Mater. Sci. Eng. 27 https://doi.org/10.1088/1361-651X/ab1efe.

Bar-Kochba, E., Scimone, M.T., Estrada, J.B., Franck, C., 2016. Strain and rate-dependent neuronal injury in a 3D in vitro compression model of traumatic brain injury. Sci. Rep. 6, 30550 https://doi.org/10.1038/srep30550.

Bardehle, S., Krüger, M., Buggenthin, F., Schwausch, J., Ninkovic, J., Clevers, H., Snippert, H.J., Theis, F.J., Meyer-Luehmann, M., Bechmann, I., Dimou, L., Götz, M., 2013. Live imaging of astrocyte responses to acute injury reveals selective juxtavascular proliferation. Nat. Neurosci. 165 (16), 580–586. https://doi.org/10.1038/nn.3371, 2013.

Binder, L.I., Frankfurter, A., Rebhun, L.I., 1985. The distribution of tau in the mammalian central nervous system. J. Cell Biol. 101, 1371–1378. https://doi.org/10.1083/JCB.101.4.1371.

Black, M.M., Slaughter, T., Moshiach, S., Obrocka, M., Fischer, I., 1996. Tau is enriched on dynamic microtubules in the distal region of growing axons. J. Neurosci. 16, 3601–3619. https://doi.org/10.1523/JNEUROSCI.16-11-03601.1996.

Dams-O'Connor, K., Gibbons, L.E., Bowen, J.D., McCurry, S.M., Larson, E.B., Crane, P.K., 2013a. Risk for late-life re-injury, dementia and death among individuals with traumatic brain injury: a population-based study. J. Neurol. Neurosurg. Psychiatry 84, 177. https://doi.org/10.1136/JNNP-2012-303938.

Dams-O'Connor, K., Spielman, L., Singh, A., Gordon, W.A., Lingsma, H.F., Maas, A.I.R., Manley, G.T., Mukherjee, P., Okonkwo, D.O., Puccio, A.M., Schnyer, D.M., Valadka, A.B., Yue, J.K., Yuh, E.L., Casey, S.S., Cooper, S.R., Cheong, M., Hricik, A.J., Knight, E.E., Menon, D.K., Morabito, D.J., Pacheco, J.L., Sinha, T.K., Vassar, M.J., 2013b. The impact of previous traumatic brain injury on health and functioning: a TRACK-TBI study. J. Neurotrauma 30. https://doi.org/10.1089/NEU.2013.3049, 2014.

Fallenstein, G.T., Hulce, V.D., Melvin, J.W., 1969. Dynamic mechanical properties of human brain tissue. J. Biomech. 2, 217–226. https://doi.org/10.1016/0021-9290(69)90079-7.

Faulkner, J.R., Herrmann, J.E., Woo, M.J., Tansey, K.E., Doan, N.B., Sofroniew, M.V., 2004. Reactive astrocytes protect tissue and preserve function after spinal cord injury. J. Neurosci. 24, 2143–2155. https://doi.org/10.1523/JNEUROSCI.3547-03.2004.

Fawcett, J.W., Asher, R.A., 1999. The glial scar and central nervous system repair. Brain Res. Bull. 49, 377–391. https://doi.org/10.1016/S0361-9230(99)00072-6.

Franceschini, G., Bigoni, D., Regitnig, P., Holzapfel, G.A., 2006. Brain tissue deforms similarly to filled elastomers and follows consolidation theory. J. Mech. Phys. Solid. 54, 2592–2620. https://doi.org/10.1016/j.jmps.2006.05.004.

Giordano, C., Kleiven, S., 2014. Evaluation of axonal strain as a predictor for mild traumatic brain injuries using finite element modeling. SAE Tech. Pap. https://doi.org/10.4271/2014-22-0002, 2014-November.

Hajiaghamemar, M., Margulies, S.S., 2020. Multi-Scale White Matter Tract Embedded Brain Finite Element Model Predicts the Location of Traumatic Diffuse Axonal Injury, pp. 144–157. https://doi.org/10.1089/NEU.2019.6791. https://home.liebertpub.com/neu38.

Hajiaghamemar, M., Wu, T., Panzer, M.B., Margulies, S.S., 2020. Embedded axonal fiber tracts improve finite element model predictions of traumatic brain injury. Biomech. Model. Mechanobiol. 19, 1109–1130. https://doi.org/10.1007/S10237-019-01273-8/FIGURES/10.

Hay, J., Johnson, V.E., Smith, D.H., Stewart, W., 2016. Chronic traumatic encephalopathy: the neuropathological legacy of traumatic brain injury. Annu. Rev. Pathol. Mech. Dis. 11, 21–45. https://doi.org/10.1146/annurev-pathol-012615-044116.

Horstemeyer, M.F., Berthelson, P.R., Moore, J., Persons, A.K., Dobbins, A., Prabhu, R.K., 2019. A mechanical brain damage framework used to model abnormal brain tau protein accumulations of national football league players. Ann. Biomed. Eng. 47, 1873–1888. https://doi.org/10.1007/s10439-019-02294-1.

Johnson, V.E., Stewart, W., Smith, D.H., 2013. Axonal pathology in traumatic brain injury. Exp. Neurol., Special Issue: Axonal Degenerat. 246, 35–43. https://doi.org/10.1016/j.expneurol.2012.01.013.

Kant, A., Johnson, V.E., Arena, J.D., Dollé, J.P., Smith, D.H., Shenoy, V.B., 2021. Modeling links softening of myelin and spectrin scaffolds of axons after a concussion to increased vulnerability to repeated injuries. Proc. Natl. Acad. Sci. U.S.A. 118 https://doi.org/10.1073/PNAS.2024961118/SUPPL_FILE/PNAS.2024961118.SAPP.PDF.

Kiernan, P., Montenigro, P., Solomon, T., McKee, A., 2015. Chronic traumatic encephalopathy: a neurodegenerative consequence of repetitive traumatic brain injury. Semin. Neurol. 35, 20–28. https://doi.org/10.1055/s-0035-1545080.

Kurtoglu, E., Nakadate, H., Kikuta, K., Aomura, S., Kakuta, A., 2017. Uniaxial stretch-induced axonal injury thresholds for axonal dysfunction and disruption and strain rate effects on thresholds for mouse neuronal stem cells. J. Biomech. Sci. Eng. 12 https://doi.org/10.1299/jbse.16-00598, 16-00598-16–00598.

LaPlaca, M., Thibault, L., 1997. Anin vitro traumatic injury model to examine the response of neurons to a hydrodynamically-induced deformation. Ann. Biomed. Eng. 25, 665–677. https://doi.org/10.1007/BF02684844.

Li, Y., Li, C., Gan, C., Zhao, K., Chen, J., Song, J., Lei, T., 2019. A precise, controllable in vitro model for diffuse axonal injury through uniaxial stretch injury. Front. Neurosci. 13, 1063. https://doi.org/10.3389/FNINS.2019.01063/BIBTEX.

McKee, A.C., Cairns, N.J., Dickson, D.W., Folkerth, R.D., Keene, C.D., Litvan, I., Perl, D. P., Stein, T.D., Vonsattel, J.-P., Stewart, W., Tripodis, Y., Crary, J.F., Bieniek, K.F., Dams-O'Connor, K., Alvarez, V.E., Gordon, W.A., TBI/CTE group, the T, 2016. The first NINDS/NIBIB consensus meeting to define neuropathological criteria for the diagnosis of chronic traumatic encephalopathy. Acta Neuropathol. 131, 75–86. https://doi.org/10.1007/s00401-015-1515-z.

McKee, A.C., Stern, R.A., Nowinski, C.J., Stein, T.D., Alvarez, V.E., Daneshvar, D.H., Lee, H.-S., Wojtowicz, S.M., Hall, G., Baugh, C.M., Riley, D.O., Kubilus, C.A., Cormier, K.A., Jacobs, M.A., Martin, B.R., Abraham, C.R., Ikezu, T., Reichard, R.R., Wolozin, B.L., Budson, A.E., Goldstein, L.E., Kowall, N.W., Cantu, R.C., 2013. The spectrum of disease in chronic traumatic encephalopathy. Brain 136, 43–64. https://doi.org/10.1093/brain/aws307.

Mez, J., Daneshvar, D.H., Kiernan, P.T., Abdolmohammadi, B., Alvarez, V.E., Huber, B. R., Alosco, M.L., Solomon, T.M., Nowinski, C.J., McHale, L., Cormier, K.A., Kubilus, C.A., Martin, B.M., Murphy, L., Baugh, C.M., Montenigro, P.H., Chaisson, C. E., Tripodis, Y., Kowall, N.W., Weuve, J., McClean, M.D., Cantu, R.C., Goldstein, L. E., Katz, D.I., Stern, R.A., Stein, T.D., McKee, A.C., 2017. Clinicopathological evaluation of chronic traumatic encephalopathy in players of American football. JAMA 318, 360–370. https://doi.org/10.1001/jama.2017.8334.

Moeendarbary, E., Weber, I.P., Sheridan, G.K., Koser, D.E., Soleman, S., Haenzi, B., Bradbury, E.J., Fawcett, J., Franze, K., 2017. The soft mechanical signature of glial scars in the central nervous system. Nat. Commun. 81 (8), 1–11. https://doi.org/10.1038/ncomms14787, 2017.

Murphy, M.A., Mun, S., Horstemeyer, M.F., Baskes, M.I., Bakhtiary, A., LaPlaca, M.C., Gwaltney, S.R., Williams, L.N., Prabhu, R.K., 2018. Molecular dynamics simulations showing 1-palmitoyl-2-oleoyl-phosphatidylcholine (POPC) membrane mechanoporation damage under different strain paths. J. Biomol. Struct. Dyn. 1–14. https://doi.org/10.1080/07391102.2018.1453376.

Noël, L., Kuhl, E., 2019. Modeling neurodegeneration in chronic traumatic encephalopathy using gradient damage models. Comput. Mech. 64, 1375–1387. https://doi.org/10.1007/s00466-019-01717-z.

Omalu, B.I., DeKosky, S.T., Minster, R.L., Kamboh, M.I., Hamilton, R.L., Wecht, C.H., 2005. Chronic traumatic encephalopathy in a national football league player. Neurosurgery 57, 128–134. https://doi.org/10.1227/01.NEU.0000163407.92769.

Perkins, R.A., Bakhtiarydavijani, A., Ivanoff, A.E., Jones, M., Hammi, Y., Prabhu, R.K., 2022. Assessment of brain injury biomechanics in soccer heading using finite element analysis. Brain Multiphys. 3, 100052 https://doi.org/10.1016/J.BRAIN.2022.100052.

Perkins, R.A., Bakhtiarydavijani, A., Prabhu, R.K., 2023. Assessment of soccer ball inflation pressurizations and risk of brain injury. ASME Int. Mech. Eng. Congr. Expo. Proc. 4 https://doi.org/10.1115/IMECE2022-89701.

Pfister, B.J., Weihs, T.P., Betenbaugh, M., Bao, G., 2003. An in vitro uniaxial stretch model for axonal injury. Ann. Biomed. Eng. 31, 589–598. https://doi.org/10.1114/1.1566445.

Pudenz, R.H., Shelden, C.H., 1946. The lucite calvarium—a method for direct observation of the brain. J. Neurosurg. 3, 487–505. https://doi.org/10.3171/jns.1946.3.6.0487.

Rashid, B., Destrade, M., Gilchrist, M.D., 2014. Mechanical characterization of brain tissue in tension at dynamic strain rates. J. Mech. Behav. Biomed. Mater. 33, 43–54. https://doi.org/10.1016/J.JMBBM.2012.07.015.

Rashid, B., Destrade, M., Gilchrist, M.D., 2013. Mechanical characterization of brain tissue in simple shear at dynamic strain rates. J. Mech. Behav. Biomed. Mater. 28, 71–85. https://doi.org/10.1016/j.jmbbm.2013.07.017.

Rashid, B., Destrade, M., Gilchrist, M.D., 2012. Mechanical characterization of brain tissue in compression at dynamic strain rates. J. Mech. Behav. Biomed. Mater. 10, 23–38. https://doi.org/10.1016/j.jmbbm.2012.01.022.

Rolls, A., Shechter, R., Schwartz, M., 2009. The bright side of the glial scar in CNS repair. Nat. Rev. Neurosci. 103 (10), 235–241. https://doi.org/10.1038/nrn2591, 2009.

Sahoo, D., Deck, C., Willinger, R., 2016. Brain injury tolerance limit based on computation of axonal strain. Accid. Anal. Prev. 92, 53–70. https://doi.org/10.1016/j.aap.2016.03.013.

Singh, A., Kallakuri, S., Chen, C., Cavanaugh, J.M., 2009. Structural and Functional Changes in Nerve Roots Due to Tension at Various Strains and Strain Rates: an In-Vivo Study, pp. 627–640. https://doi.org/10.1089/NEU.2008.0621 home.liebertpub.com/neu26.

Skotak, M., Wang, F., Chandra, N., 2012. An in vitro injury model for SH-SY5Y neuroblastoma cells: effect of strain and strain rate. J. Neurosci. Methods 205, 159–168. https://doi.org/10.1016/j.jneumeth.2012.01.001.

Smith, M., 2020. ABAQUS/Standard User's Manual, Version 6.20. Dassault Systèmes Simulia Corp, Providence, RI.

Tang-Schomer, M.D., Patel, A.R., Baas, P.W., Smith, D.H., Smith, D., 2010. Mechanical breaking of microtubules in axons during dynamic stretch injury underlies delayed elasticity, microtubule disassembly, and axon degeneration. Faseb. J. 24, 1401–1410. https://doi.org/10.1096/FJ.09-142844.

Tse, K.M., Lim, S.P., Tan, V.B.C., Lee, H.P., 2015. A Review of Head Injury and Finite Element Head Models. Openscienceonline.Com/1, 28, 7370142.

Vo, Anh T.N., Murphy, M.A., Phan, P.K., Prabhu, R.K., Stone, T.W., 2023. Effect of force field resolution on membrane mechanical response and mechanoporation damage under deformation simulations. Mol. Biotechnol. https://doi.org/10.1007/s12033-023-00726-x.

Vo, A.T.N., Murphy, M.A., Phan, P.K., Stone, T.W., Prabhu, R.K., 2023. Molecular dynamics simulation of membrane Systems in the context of traumatic brain injury. Curr. Opin. Biomed. Eng. 100453 https://doi.org/10.1016/j.cobme.2023.100453.

Wang, H., Song, G., Chuang, H., Chiu, C., Abdelmaksoud, A., Ye, Y., Zhao, L., 2018. Portrait of glial scar in neurological diseases. Int. J. Immunopathol. Pharmacol. 31, 1–6. https://doi.org/10.1177/2058738418801406.

Zhang, L., Yang, K.H., King, A.I., 2004. A proposed injury threshold for mild traumatic brain injury. J. Biomech. Eng. 126, 226–236. https://doi.org/10.1115/1.1691446.